




Enhanced out-coupling efficiency in OLEDs using ZnS nanodots

Il-Ji Bae, Dasom Song, Dang Mo Yoon, Deepak Ghimire, Miyoung Kim, Bum-Joo Lee, Byung Yun Joo, Ju Hwan Choi, Jin-Koog Shin & Jae-Wook Kang

To cite this article: Il-Ji Bae, Dasom Song, Dang Mo Yoon, Deepak Ghimire, Miyoung Kim, Bum-Joo Lee, Byung Yun Joo, Ju Hwan Choi, Jin-Koog Shin & Jae-Wook Kang (2016) Enhanced out-coupling efficiency in OLEDs using ZnS nanodots, *Molecular Crystals and Liquid Crystals*, 635:1, 181-189, DOI: [10.1080/15421406.2016.1201409](https://doi.org/10.1080/15421406.2016.1201409)


To link to this article: <http://dx.doi.org/10.1080/15421406.2016.1201409>

 View supplementary material 

 Published online: 01 Nov 2016.

 Submit your article to this journal 

 Article views: 13

 View related articles 

 View Crossmark data 

Enhanced out-coupling efficiency in OLEDs using ZnS nanodots

Il-Ji Bae^a, Dasom Song^{a,d}, Dang Mo Yoon^b, Deepak Ghimire^a, Miyoung Kim^a, Bum-Joo Lee^a, Byung Yun Joo^c, Ju Hwan Choi^a, Jin-Koog Shin^a, and Jae-Wook Kang^d

^aKorea Printed Electronics Center, Korea Electronics Technology Institute, Jeonju, Korea; ^bDivision of Microelectronics and Display Technology, Wonkwang University, Iksan, Korea; ^cSchool of Mechanical Engineering, Korea University of Technology & Education, Cheonan, Korea; ^dDepartment of Flexible and Printable Electronics, Chonbuk National University, Jeonju, Korea

ABSTRACT

We demonstrated highly efficient OLEDs by incorporating ZnS nanodots on top of a glass substrate via a chemical bath deposition process. The device efficiency of OLEDs with ZnS nanodot arrays was 1.26 times higher than that of OLEDs without ZnS. This enhancement in device efficiency is attributed to the improved light out-coupling efficiency that is enabled by the improved optical performance of nanodot arrays, which results from their high refractive index and optical transmittance in the visible wavelength.

KEYWORDS

High refractive index; ZnS; Hemisphere; Nanodot; Organic light-emitting diode

Introduction

Organic light-emitting devices (OLEDs) are attractive as potential next generation displays in flexible and transparent devices, as well as in solid-state lighting [1–5]. The external quantum efficiency (η_{ex}) of OLEDs is governed by the product of the internal quantum efficiency and the light out-coupling factor. This can be expressed by the equation $\eta_{ex} = \alpha \gamma \eta_r \Phi_{PL}$, where α is the light out-coupling factor, γ is the probability of carrier recombination, η_r is the production efficiency of excitons, and Φ_{PL} is the absolute PL quantum yield of the emitter. The η_r was recently improved by nearly 100% by using phosphorescent dyes (as opposed to fluorescent dyes), which are able to harvest both singlet and triplet excitons [6–7]. The refractive indices of the various layers in the OLED structures are significantly larger than that of air. The refractive indices (n) are as follows: ~ 1.5 for the glass substrate, ~ 1.9 for indium tin oxide (ITO), and ~ 1.7 for the organic materials. Therefore, a relatively small value of α ($\alpha \approx 1/2n^2 \approx 20\%$) of the generated light can escape to the outside of the substrate. Recently, there have been reports of a calculated α over 30% [8–9]. The remainder of the light is confined in the glass substrate by the total internal reflection ($\sim 30\%$ of the emitted light) or trapped in the waveguide modes that are associated with the ITO and the organic layers ($\sim 50\%$ of the emitted light), which possess high refractive indices [10]. Therefore, the light out-coupling factor can be improved if this confined and trapped light is redirected toward the surface that is normal to the OLED structure. Recently, a variety of techniques, such as macroscopic lenses, micro-lenses, Bragg reflectors, and substrate roughening, have been demonstrated to improve the out-coupling efficiency of OLEDs. However, these technologies have yet to be applied in industry due to

CONTACT Miyoung Kim ✉ miy1kim@keti.re.kr; Jae-Wook Kang ✉ jwkang@jbnu.ac.kr

Color versions of one or more of the figures in the article can be found online at www.tandfonline.com/gmcl.

© 2016 Taylor & Francis Group, LLC

their complicated processes (which are unsuitable for mass production) and their propensity to discolor polymer films when used in OLED lighting [11–14].

In this paper, we report the enhanced light out-coupling efficiency of OLEDs that is achieved by incorporating high-refractive index ZnS nanodots onto the glass side of the ITO substrate. ZnS, which is a wide direct band gap semiconductor with a high refractive index ($n \sim 2.35$), is a promising material for detectors, emitters, and modulators in optoelectronics [15]. Recently, ZnS films have been used as reflectors and dielectric filters due to the high value of their refractive index, as well as their high transmittance in the visible region [16]. The chemical bath deposition (CBD) technique, which is a cost-effective and commercially-available approach, is well-suited for depositing ZnS films on semiconductors or glass substrates. CBD is a well-known process that represents one of the least expensive methods that can be used to deposit large-area ZnS thin films for photovoltaic applications [17–21]. In this study, ZnS nanodot arrays were deposited on the glass side of ITO substrates for light out-coupling of OLEDs. The device efficiency of OLEDs with these ZnS nanodot arrays was 1.26 times higher than that of OLEDs without ZnS. This enhancement in the device efficiency can be attributed to the improved light out-coupling efficiency that is enabled by the improved optical performance of nanodot arrays, which results from their high refractive index and optical transmittance in the visible wavelength.

Experimental details

In order to calculate the light extraction effect on the glass substrate with ZnS nanodot arrays, we used the simulation program Light Tools (Synopsys Optical Solution, USA). Light Tools is a well-known 3D optical engineering and design software based on Monte Carlo analysis. The device structure is ZnS ($n = 2.15$) / glass (thickness = 5 mm, $n = 1.48$) / ITO (thickness = 150 nm, $n = 1.86$) / HTL (thickness = 60 nm, $n = 1.82$) / EML (thickness = 30 nm, $n = 1.74$) / ETL (thickness = 30 nm, $n = 1.66$) / EIL (thickness = 3 nm, $n = 1.66$) / cathode (Al), where HTL, EML, ETL, and EIL are the hole-transporting layer, emission layer, electron-transporting layer, and electron-injection layer, respectively. For simplicity, the wavelength of light used for this simulation was 550 nm, which is the peak wavelength of the EL spectrum of the OLEDs. ZnS nanodot arrays are monodisperse with a fill factor of 0.34. The fill factor is defined as the ratio of the area covered by the nanodot arrays with respect to the area of the substrate [22]. The diameter (D) of ZnS nanodots was increased from 110 nm to 290 nm at intervals of 30 nm.

It is well-known that the CBD method can be used to deposit thin films for large area substrates via a low-cost and simple process. In the CBD method, a soluble salt of the required metal is dissolved in an aqueous solution to release cations. A suitable source compound, which decomposes in the presence of hydroxide ions and releases the requisite anions, provides the non-metallic element. The anions and cations then react to form the desired compound. ZnS thin films can be prepared by the decomposition of thiourea in an alkaline solution containing a zinc salt [23]. Figure S1 shows a schematic diagram for the CBD method. Depositions take place on the glass side of ITO substrates to grow the ZnS nanodot arrays. These were cleaned with detergent in an ultrasonic cleaner and dried with N_2 . The solutions were prepared using analytical-grade reagents ($ZnCl_2$, $(NH_2)_2CS$, and 28.0–30.0% NH_4OH). ZnS nanodot arrays were chemically grown on glass using an aqueous solution containing $ZnCl_2$ (0.025 M), NH_4OH (1 M), and $(NH_2)_2CS$ (0.1 M) at 65–90°C. The surface morphology of the as-deposited ZnS nanodot arrays was studied using a focused ion beam (FEI Quanta 3D FEG). Detailed chemical reactions for the formation of ZnS nanodot arrays are given in

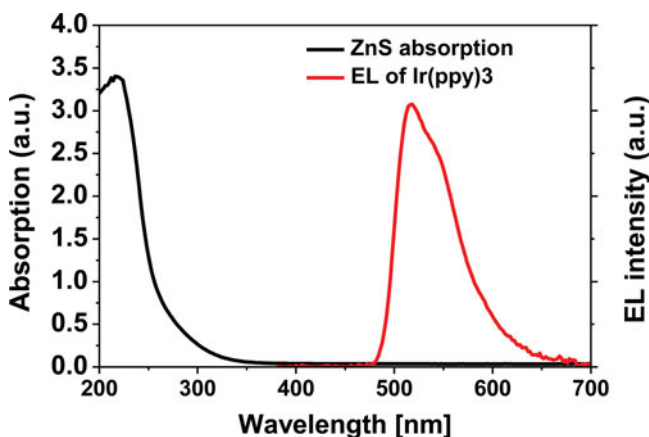


Figure 1. UV-Vis absorption spectrum of ZnS and EL intensity of green OLED devices.

the literature [21]. We fabricated two types of ZnS nanodot arrays using the CBD method. For type I, after growing the seed layer at 90°C for 3 min (to produce arrays with a diameter (D) of 40 nm), ZnS arrays were grown at 65°C for 60 to 300 min; this formed arrays with $D = 75$ to $D = 210$ nm, respectively. For type II, ZnS arrays were grown at 90°C for 30 to 120 min, resulting in arrays with $D = 55$ to $D = 100$ nm, respectively.

The EL devices were fabricated on pre-cleaned and plasma-treated ITO-coated glass substrates [24–27]. The samples were then brought into a thermal evaporation chamber (SUNICEL 200Plus), which was inside of a glove box filled with N_2 . OLEDs were fabricated, based on our standard green phosphorescent device, with the structure of HIL (LHI-001, 100 nm) / HTL (LHT-259, 40 nm) / EML (PGH02 doped 8 wt.% Ir(ppy)₃, 30 nm) / ETL (Bebq₂, 30 nm) / EIL (Liq, 3 nm) / Al (100 nm), where Ir(ppy)₃ is fac-tris(2-phenylpyridine) iridium, Beq₂ is bis(10-hydroxybenzo[h]quinolino)beryllium, and Liq is 8-hydroxyquinolino-lithium. The HIL, HTL, host of the EML, and EIL were purchased from Duksan Hi-Metal Co. Ltd. All organic layers were grown by thermal evaporation at a base pressure of approximately 7×10^{-7} torr with the following deposition rates: 1.0 Å/s for the HIL, HTL, ETL, and host of the EML; 0.8 Å/s for dopant of the EML; 0.1 Å/s for the EIL; and 2 Å/s for the Al electrode. The film thicknesses of all layers were determined with an Alpha-Step instrument (KLA Tencor P-16+). The current density–voltage (J – V) and luminance–voltage (L – V) characteristics were recorded with a source-measure unit (Keithley 236) and a calibrated photodiode (Photo Research Inc., PR-670). The angular distribution of the EL intensity was measured by a source meter (Keithley 2400), rotation stage, and fiber optic spectrometer (Ocean Optics S2000). The UV-Vis absorption spectrum of ZnS was measured by a UV-Vis spectrophotometer (Dong-il SHIMADZU Corp., UV-2600).

Results and discussion

UV absorption

In this experiment, we made light extraction structures on the glass side of ITO substrates with ZnS nanodot arrays using the CBD process. Figure 1 shows the UV-Vis absorption spectrum of the ZnS nanodot arrays and the EL spectrum of Ir(ppy)₃-based phosphorescent OLEDs. The results show that the absorption spectrum of ZnS has no influence on the light

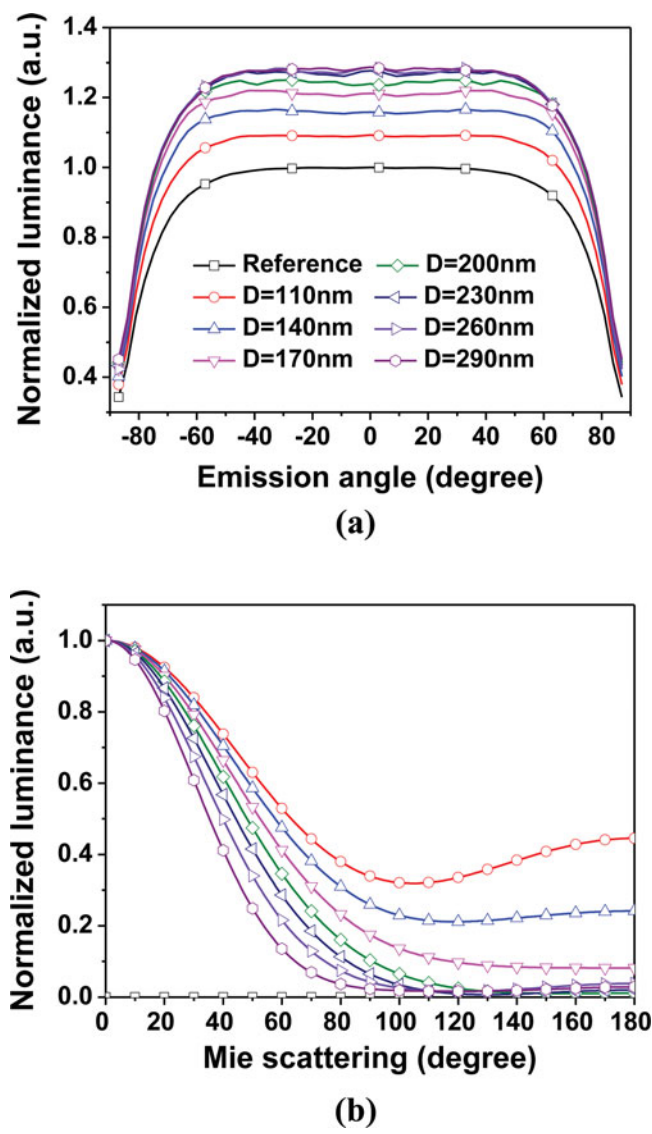


Figure 2. Simulation results of OLED devices with ZnS nanodot arrays on glass substrates. (a) Normalized luminance depending on the emission angle. (b) Normalized luminance depending on the Mie scattering.

out-coupling of the emitted wavelength (around 520 nm). Therefore, we expect that the ZnS nanodots will not interrupt light out-coupling.

Simulation of OLED devices with ZnS nanodot arrays

Figure 2(a) shows the simulation results of the normalized luminance as a function of the emission angle of OLED devices with ZnS nanodot arrays with various diameters. Simulations were performed by varying the diameter of the ZnS from 110 nm to 290 nm at intervals of 30 nm. OLEDs with ZnS nanodot arrays with a diameter of 260 nm show the maximum luminance, which is 1.28 times higher than that of the reference without ZnS. Figure 2(b) shows the normalized luminance as a function of the Mie scattering angle for ZnS arrays with $D = 110$ nm to $D = 290$ nm. The OLEDs with ZnS arrays with D between 110 and 170 nm

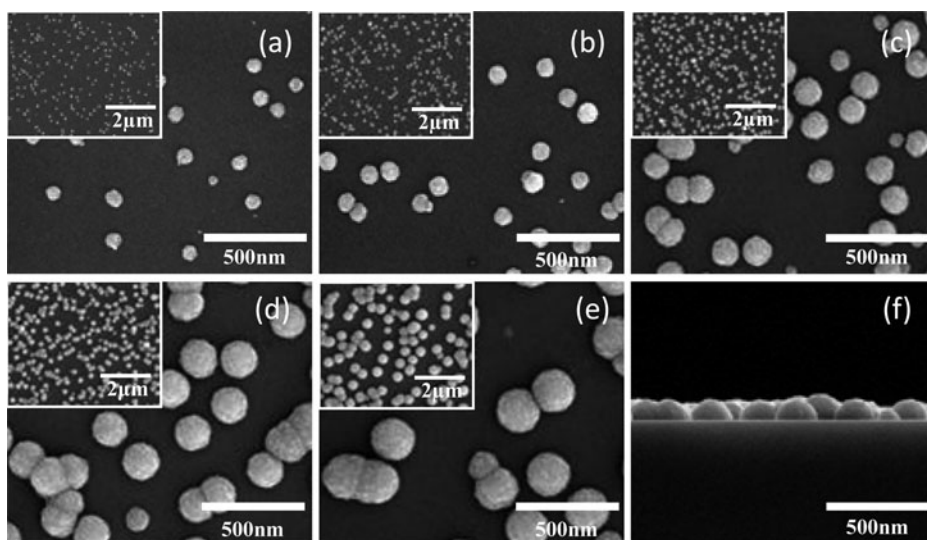


Figure 3. SEM images of ZnS nanodot arrays made by type I process conditions with various deposition times at 65°C: (a) 60 min ($D = 75$ nm, $FF = 0.05$), (b) 120 min ($D = 88$ nm, $FF = 0.10$), (c) 180 min ($D = 135$ nm, $FF = 0.23$), (d) 240 min ($D = 180$ nm, $FF = 0.34$), (e) 300 min ($D = 210$ nm, $FF = 0.42$), and (f) cross-sectional view of (e).

show higher back scattering luminance (for $D = 110$ nm, 33.5% and $D = 170$ nm, 9.7%) than those of OLEDs with D between 200 and 290 nm (for $D = 200$ nm, 2.4% and $D = 290$ nm, 1.6%) at an angle of 120°. On the basis of these results, ZnS nanodots with a larger diameter decreased the back side Mie scattering of the devices, thereby increasing the front side luminance of the emitted light.

Characteristics of OLED devices

Figures 3 and 4 show SEM images of ZnS nanodot arrays deposited by the type I and type II conditions, respectively. The diameter of ZnS nanodots is proportional to the growth time from $D = 75$ to $D = 210$ nm and from $D = 55$ to $D = 100$ nm, for 300 and 100 min, respectively. In addition, the fill factor (FF) also increased with longer growth times. The ZnS diameter of type II nanodots at a higher deposition temperature ($\sim 90^\circ\text{C}$) was larger than that of type I nanodots deposited at 65°C. As a shown in Figure 4(f), the cross-sectional view of the

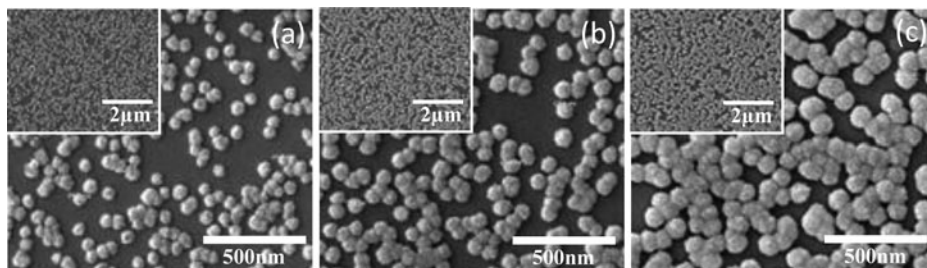


Figure 4. SEM images of ZnS nanodot arrays made by type II process conditions with various deposition times at 90°C: (a) 30 min ($D = 55$ nm, $FF = 0.46$), (b) 60 min ($D = 80$ nm, $FF = 0.54$), and (c) 120 min ($D = 100$ nm, $FF = 0.65$).

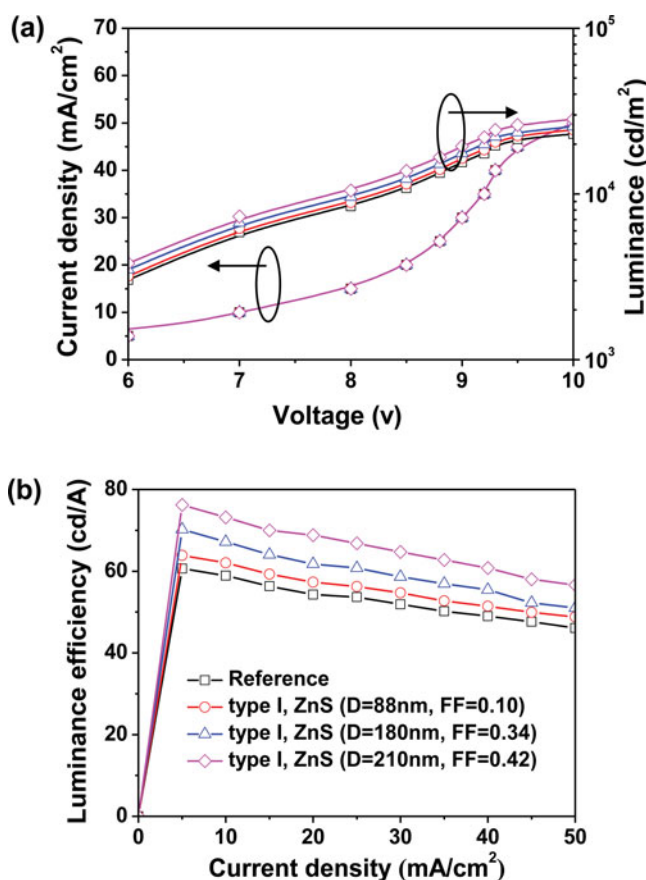


Figure 5. Characteristics of OLEDs with ZnS nanodot arrays deposited by type I process conditions: (a) voltage-current density-luminance characteristics and (b) luminance efficiency-current density characteristics.

deposited ZnS shows nanodots that were 102 nm in height, possessed a hemispherical shape, and were 210 nm in diameter.

Figures 5 and 6 show characteristics of the OLEDs with ZnS nanodot arrays deposited by the type I and type II conditions, respectively. As shown in Figures 5(a) and 6(a), all devices have approximately identical voltage-current density characteristics. For the type I-based OLEDs shown in Figure 5, the device performance was improved by increasing the D and FF of ZnS nanodots. The luminance of the device with ZnS nanodots (FF = 0.42 and D = 210 nm) is 1.26 times higher than that of the reference (without ZnS) at a current density of 5 mA/cm². As a result, the luminance efficiency is increased from 60.6 cd/A up to 76.2 cd/A, resulting in an enhancement that is similar to the results predicted via simulation (an improvement by a factor of 1.28). For the type II-based OLEDs shown in Figure 6, the device efficiency was increased to 66.4 cd/A (at FF = 46) and then decreased to 61.0 cd/A as the FF continued to increase. Figure 7 shows the efficiency enhancements of OLEDs at a current density of 5 mA/cm², normalized to that of the reference, as a function of the FF for type I and type II devices. This shows that the efficiency enhancement was maximized around an FF of 0.4; the efficiency then gradually decreased due to a drop in the transmittance. Above a FF of 0.5, the ZnS nanodots form a thin film, resulting in a decreased transmittance in the visible wavelength (Figure S2). The variation of the emission intensity as a function of the viewing

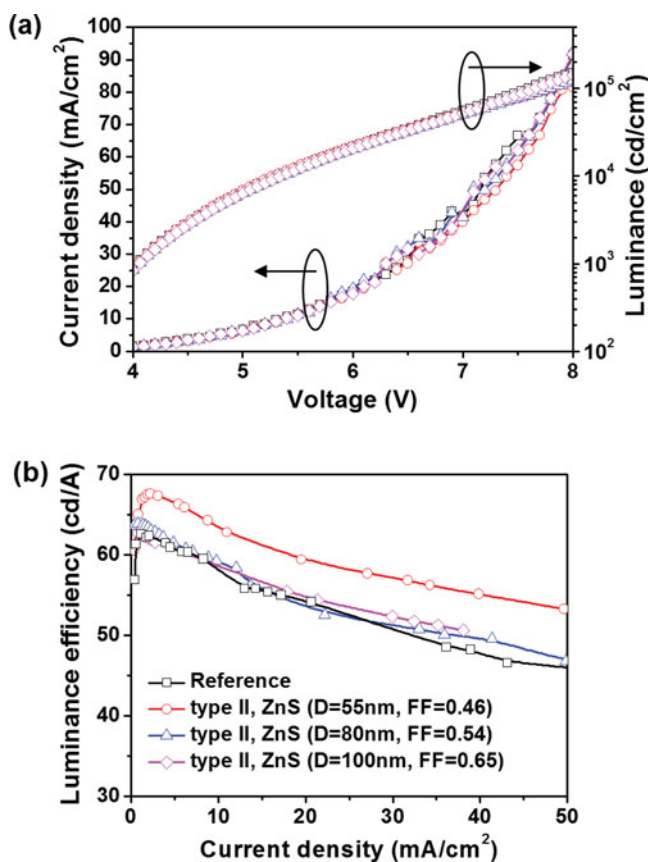


Figure 6. Characteristics of OLEDs with ZnS nanodot arrays deposited by type II conditions: (a) voltage-current density-luminance characteristics and (b) luminance efficiency-current density characteristics.

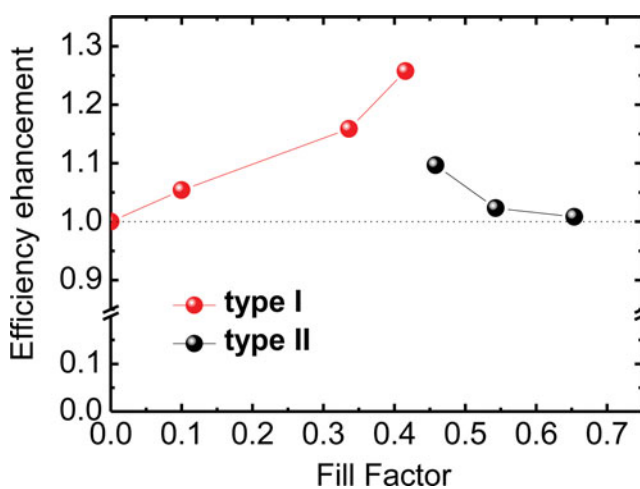


Figure 7. Fill factor-dependent efficiency enhancement of OLEDs normalized to that of the reference device at a current density of 5 mA/cm².

angle was measured by using a rotating stage and an optical fiber at $1,000 \text{ cd/m}^2$ (Figure S3). The reference OLED shows a Lambertian pattern for the emission intensity as a function of the viewing angle, as expected. The radiation profile of OLEDs with ZnS nanodot arrays is almost the same as the Lambertian emission.

Summary

In summary, we demonstrated an enhanced out-coupling efficiency in OLEDs that incorporated ZnS nanodot arrays. As a result, the device efficiency was 1.26 times higher than that of a reference device without ZnS. ZnS nanodots were fabricated via the chemical bath deposition process. These were easily manufactured on glass substrates of a much larger scale than what has been done for polymer (e.g., methyl methacrylate) micro-lens arrays (or nano-lens arrays) [28]. Additionally, the hemisphere shape of the ZnS is not easily deformed due to the material's high hardness (relative to what is used for micro-lens array films). Therefore, due to the facile nature, low cost, and high reliability of this process, we expect that this technique can be applied for the mass production of OLEDs.

Acknowledgments

This research was supported by the Fusion and Complex Technique Development Project (S2171611), by the Jeonbuk Research & Development Program funded by Jeonbuk Province (20140310-A-001), and in part by the Basic Science Research Program through the National Research Foundation of Korea funded by the Ministry of Science, ICT & Future Planning (NRF-2014R1A1A1003341).

References

- [1] C. W. Tang; S. A. Vanslyke. *Appl. Phys. Lett.*, 1987, 51, 913–915.
- [2] J. Shi; C. W. Tang. *Appl. Phys. Lett.*, 1997, 70, 1665–1667.
- [3] G. Rajeswaran; M. Itoh; M. Boroson; S. Barry; T. K. Hatwar; K. B. Kahen; K. Yoneda; R. Yokoyama; T. Yamada; N. Komiya; H. Kanno; H. Takahashi. *SID Symposium Digest of Technical Papers, Long Beach, California, USA*, May 16–18, 2000, 31, 947.
- [4] Y. Wang; N. Herron; V. V. Grushin; D. LeCloux; V. Petrov. *Appl. Phys. Lett.*, 2001, 79, 449–451.
- [5] L. S. Hung; C. W. Tang; M. G. Mason; P. Raychaudhuri; J. Madathil. *Appl. Phys. Lett.*, 2001, 78, 544–546.
- [6] C. Adachi; M. A. Baldo; M. E. Thompson; S. R. Forrest. *J. Appl. Phys.*, 2001, 90, 5048.
- [7] Y. Kawamura; K. Goushi; J. Brooks; J. J. Brown; H. Sasabe; C. Adachi. *Appl. Phys. Lett.*, 2005, 86, 071104.
- [8] S.-Y. Kim; J. J. Kim. *Org. Electron.*, 2010, 11, 1010.
- [9] C.S. Kim; M. Kim; D. C. Larrabee; I. Vurgaftman; J. R. Meyer; S. H. Lee; Z. H. Kafafi. *J. Appl. Phys. Lett.*, 2009, 106, 113105.
- [10] K. Saxena; V. K. Jain; D. S. Mehta. *Opt. Mater.*, 2009, 32, 221.
- [11] C. F. Madigan; M.-H. Lu; J. C. Sturm. *Appl. Phys. Lett.*, 2000, 76, 1650.
- [12] S. Moller; S. R. Forrest. *J. Appl. Phys.*, 2002, 91, 3324.
- [13] S. M. Jeong; Y. Takanishi; K. Ishikawa; H. Takezoe. *Jpn. J. Appl. Phys.*, 2006, Part 2 45, L737.
- [14] R. Windisch; P. Heremans; A. Knobloch; P. Kiesel; G. H. Dohler; B. Dutta; G. Borghs. *Appl. Phys. Lett.*, 1999, 74, 2256.
- [15] B. Elidrissi; M. Addou; M. Regragui; A. Bougrine; A. Kachouane; J.C. Berne 'de. *Mater. Chem. Phys.*, 2001, 68, 175–179.
- [16] J.A. Ruffner; M.D. Hilmel; V. Mizrahi; G.I. Stegeman; U. Gibson. *J. Appl. Opt.*, 1989, 28, 5209.
- [17] C. J. Yang; C. L. Lin; C. C. Wu; Y. H. Yeh; C. C. Cheng; Y. H. Kuo; T. H. Chen. *Appl. Phys. Lett.*, 2005, 87, 143507.

- [18] Q. Li. *Self-Organized Organic Semiconductors; From Materials to Device Application*; John Wiley & Sons, 2011.
- [19] Q. Li *Liquid crystals beyond displays: chemistry, physics, and applications*; John Wiley & Sons, 2012.
- [20] A. Uchiyama; T. Yatabe. Proceedings of the 7th International Display Workshop, Kobe, Japan, November 29–December 1, 2000.
- [21] A. Uchiyama; T. Yatabe. SID Symposium Digest of Technical Papers, San Jose, California, USA, June 5–7, 2001.
- [22] D. H. Hwang; O. T. Kwon; W. J. Lee; J. W. Hong; T. W. Kim. *Status Solidi A211*, 2014, No. 8, 1773–1777.
- [23] U. Gangopadhyay; K. H. Kim; D. Mangalaraj; J. Yi. *Applied Surface Science*, 2004, 230, 364–370
- [24] V. Bulovic; G. Gu; P. E. Burrows; S. R. Forrest; M. E. Thompson. *Nature*, 1996, 380, 29.
- [25] G. Parthasarathy; P. E. Burrows; V. Khalfin; V. G. Kozlov; S. R. Forrest. *Appl. Phys. Lett.*, 1998, 72, 2138–2140
- [26] T. Sasaoka; M. Sekiya; A. Yumoto; J. Yamada; T. Hirano; Y. Iwase; T. Yamada; T. Ishibashi; T. Mori; M. Asano; S. Tamura; T. Urabe. SID Symposium Digest of Technical Papers, San Jose, California, USA, June 5–7, 2001.
- [27] M. H. Lu; M. S. Weaver; T. X. Zhou; M. Rothman; R. C. Kwong; M. Hack; J. J. Brown. *Appl. Phys. Lett.*, 2002, 81, 3921–3923.
- [28] P. O'Brien; J. McAleese. *J. Mater. Chem.*, 1998, 8(11), 2309–2314.